Passive thermal regulation approach for Algofilm © photobioreactor through phase change

Kashif Mangi, Zakaria Larbi, Jack Legrand, Jeremy Pruvost, El-Khider Si-Ahmed

Passive thermal regulation approach for Algofilm © photobioreactor through phase change

Kashif Hussain Mangi[a,b], *Zakaria Larbi*[c], *Jack Legrand*[a], *Jérémy Pruvost*[a], *El-Khider Si-Ahmed*[a,*]

[a] *University of Nantes, ONIRIS, CNRS, GEPEA, UMR-6144, 37 Bd de l'université BP406, 44602 Saint-Nazaire, France*
[b] *Department of Chemical Engineering, Quaid-e-Awam University of Engineering, Sciences and Technology, Nawabshah, Pakistan*
[c] *Laboratoire de Mécanique des Fluides Théorique et Appliquée, Département d'Energétique et de Mécanique des Fluides, Faculté de Physique, USTHB, B.P. 32, El-Alia 16111, Algeria*

Keywords:
Algofilm © Photobioreactor
Passive thermal regulation
Evaporation
Condensation

A B S T R A C T

This study deals with the development of a self-sustained passive thermal regulation technique in Algofilm © solar photobioreactor. The reported experimental investigation includes, the evaluation of an average equivalent condensate film thickness, in indoor operating conditions, as function of the flowing liquid T_l and ambient T_{amb} temperatures, inclination angle ϕ as well as air flowrate. For instance, an average condensate film thickness of 2.2 ± 0.2 mm at $T_l = 50\,^{\circ}$C, for liquid flow rate of 0.08 l/s and $\phi = 4^{\circ}$ in steady state conditions was recorded. Furthermore, a correlation estimating the condensation rate as function of the flowing liquid and ambient temperatures, was developed. A theoretical, heat and mass transfer model was proposed and validated with the indoor experimental results. The numerical predictions of the model adapted to a simulated sunny day were in good agreement with the experimental recordings. This validation evidenced the model applicability to real solar conditions, where an accurate evaluation of the condensed water is required for predicting the infrared filtration.

1. Introduction

Microalgae are unicellular microorganisms that can convert sunlight into biochemical energy via the process of photosynthesis. It is a promising feedstock for bulk commodities like chemicals, food, nutraceutical, pharmaceutical industries and bio-fuels (Litchman and Klausmeier, 2001; Spolaore et al., 2006; Axelsson et al., 2012; Draaisma et al., 2013). Microalgae is becoming a prominent technology for wastewater treatment (Derakhshan et al., 2019; Xie et al., 2019; Yang et al., 2019; Luo et al., 2021), and has been considered as one of the sustainable solutions towards CO_2 control and capture (Al Ketife et al., 2016) to counter the global warming and climatic change (Zhao et al., 2019).

Open raceways and closed photobioreactors are mainly considered for microalgae production. However, the open systems are applicable to few microalgae species, whereas the closed systems are relevantly preferred due to controlled and isolated operation as well as their capability to produce more microalgae species (Benemann, 2013).

Numerous photobioreactors have been developed to produce various strains of microalgae and optimize biomass productivity and photosynthesis efficiency (Pruvost et al., 2006; Goetz et al., 2011; de Jesus and Maciel Filho, 2017; Solimeno et al., 2017; Deprá et al., 2019).

The volumetric productivity enhancement of microalgae cultivation depends on several factors, including solar radiation, temperature, nutrient feeding procedures, pH regulation,

* Corresponding author.
E-mail address: el-khider.si-ahmed@univ-nantes.fr (E.-K. Si-Ahmed).
https://doi.org/10.1016/j.cherd.2021.02.013

Nomenclature

Accents

$\bar{x}$	Average quantity

Greek symbols

β	Correction factor, –
δ	Film thickness, m
ρ	Density, kg/m^3

Roman symbols

$\dot{m}$	Mass flux, kg/s
D_v	Binary diffusion coefficient, m^2/s
H	Enthalpy, J
h	Heat transfer coefficient, w/m^2 K
k	Thermal conductivity, w/m K
L	Length, m
L_{evap}	Latent heat, kJ/kg
Nu	Nusselt number, –
p	Partial vapor pressure, Pa
Q	Heat flux, J/s
Ra	Rayleigh number, –
Re	Reynold's number, –
S	Surface, m^2
T	Temperature, K
t	Time, s
W	Width, m
U	Velocity, m/s
Y	Vapor mass fraction, –

Superscripts

0	Initial conditions
amb	Ambient
b	Bottom
c	Critical
cond	Condensation
conv	Convection
evap	Evaporation
fc	Forced convection
ha	Humid air
i	Subsystem
in	Input flux
l	Liquid
out	Output flux
r	Residence
v	Vapor
w	Condensate
w/g	Glass-water

Acronyms

ϕ	Inclination angle
PBR	Photobioreactor
PEC	Passive evaporative cooling

mixing (Pruvost et al., 2016), and gas hold up (Sabri et al., 2019). Temperature and light are important factors to control the biomass and lipid production in algae (Ugwu et al., 2008; Pruvost et al., 2012; Xu et al., 2009; Solimeno et al., 2017; Shuba and Kifle, 2018). Algal growth rates increases with temperature up to an optimum range Muller-Feuga et al. (1998). The optimum light (Cheng et al., 2020) and temperature (Singh and Singh, 2015) were studied for the maximum growth of different species of algae. Ras et al. (2013) reported the optimum temperature ranges, to achieve maximum microalgae productivity, for different types of microalgae were 25, 25, 40 °C respectively for psychrophilic (Asterionella formosa), mesophilic and thermophilic (Chaetoceros, Anacystis nidulans) species.

The estimation of microalgae production is quite difficult in outdoor systems (Mata et al., 2010; Béchet et al., 2014). For instance, the temperature cannot be easily controlled at outdoor scale, because algae species experience significant temperature change during varied weather conditions such as cloudy conditions, Day/Night cycle and seasonal variations (Béchet et al., 2010; Pruvost et al., 2019).

Overheating of photobioreactors is an unavoidable challenge for microalgal mass production, resulting in low photosynthetic efficiency and low biomass productivity (Pruvost et al., 2017, 2019). Microalgae production requires thermal regulations in outdoor conditions (Bechet, 2014; Nwoba et al., 2019; Pruvost et al., 2019). Microalgae needs the photo-synthetically active spectrum i.e. 400–700 nm for biomass growth (Wondraczek et al., 2015; Baer et al., 2016). Therefore a substantial portion of the solar spectrum is unwanted for these solar PBRs which includes infrared and ultraviolet ranges which are the basic cause of overheating and cell-damaging on microalgae culture (Nwoba et al., 2019). Some recent researches have witnessed that microalgae culture temperature can be regulated through passive evaporating cooling (PEC) and glazing which can filter infrared spectrum (Béchet et al., 2010; Nwoba et al., 2016). Although PEC is an active thermal regulation approach but still due to cost and performance limitation, the use of PEC systems to maintain the optimum culture temperatures is not economically or environmentally sustainable. However, the glazing affects the transmission of the visible spectrum. Therefore, an innovative technology for microalgal PBR that requires less, or no, freshwater to filter the infrared spectrum will be a game-changer (Nwoba et al., 2019).

On the passive thermal regulation for a semi-buried open raceway, Pruvost et al. (2019) has developed a thermal model to cultivate microalgae and achieved very good agreement with experimental results for temperatures. However, the simultaneous heat and mass transfer study for any open or closed PBR system, up to our knowledge, has not been reported yet. In solar photobioreactors, evaporation is often observed during microalgae production (Torzillo et al., 1986; Moheimani et al., 2011; Hindersin et al., 2013), also in Algofilm © photobioreactor (Goetz et al., 2011), which can be driven to develop condensate droplets or a film at the inner surface of the top cover. The developed condensate film can absorb infrared radiations reducing then the overheating in the Algofilm © PBR. Subsequently, water (condensate) is a promising filter which can transmit the visible light, required for microalgae growth, and absorb the infrared the major cause of overheating in outdoor PBRs (Nwoba et al., 2019). For instance, Krauter (2004) used a thin water film over a photovoltaic panel and achieved a huge reduction of 22 °C in the panel temperature.

The absorption of infrared radiation is a volumetric process (Kirk, 1988), therefore, it is imperative to quantify the amount of condensate which will be developed in outdoor conditions. The estimation of condensate film is extremely complicated in outdoor condition, due to the involvement of complex phenomena such as temperature variations with simultaneous heat and mass transfer with phase change (evaporation and condensation), in addition to solar radiation, ambient air velocity, relative humidity and the day/night cycle

(Apel and Weuster-Botz, 2015; Apel et al., 2017; Huesemann et al., 2017). Therefore, an optimized study cannot be carried out to establish a robust basis for modelling purposes.

Understanding and quantifying the phase change phenomena at controlled indoor conditions will constitute the basis for the estimation of condensate in outdoor conditions. For that purpose, this paper aims to build up a theoretical and experimental study which can be further used for outdoor conditions. The experimental study is conducted on indoor lab-scale Algofilm © prototype with the constant operating parameters to investigate the influence of flowing liquid temperature, air injection, and the inclination angle of the cover on the hourly condensation mass flux. A theoretical study was also carried out by considering the global simultaneous heat and mass transfer model with phase change.

2. Experimental setup and model considerations

2.1. *Experimental setup*

The lab-scale Algofilm © photobioreactor of the GEPEA laboratory, as shown in Fig. 1a, has a 0.33 m^2 surface area and it is mainly made up of stainless steel and aluminum with a transparent cover of Plexiglas. This prototype has an ability to be inclined up to 65°, which made possible the collection of condensed mass that could be compared with the numerical predictions. The Algofilm © PBR was divided into four subsystem including bottom plate (i.e stainless steel), flowing liquid on bottom plate, condensate as well as the top cover plate (i.e. plexiglas), and humid air in between flowing liquid and condensate film as shown in (see Fig. 1a). All experiments were conducted in fully controlled indoor conditions such as regulated room temperature, the flowing liquid temperature was maintained constant through the external water heater, and was continuously re-circulated, at a constant volume flow rate, through an integrated pump. Liquid film was injected uniformly through a flow stabilizer at the inlet point (see Fig. 1c), which is quite effective to make a smoother and uniform flow of liquid on the bottom of Algofilm © PBR. The size and distribution of holes were already optimized on the same experimental setup in previous studies by Le Borgne (2014), Pruvost et al. (2017).

2.2. *Experimental data acquisition*

Indoor experimental setup is mainly based on the precise data acquisition regarding mass quantification and temperature distribution in every subsystem of Algofilm © PBR. A dedicated LabVIEW program was established to record the data (i.e. temperature, airflow rate etc) of each subsystem (glass-condensate film, humid air medium (inside air), flowing liquid and the bottom) as shown in Fig. 1b. The thermocouples for each sub-system are uniformly distributed on the centre in every zone (i.e., top, middle, and lower zones) see Fig. 1c (showing the thermocouples distribution for the flowing liquid sub-system). The horizontal surface of exchange is 30×100 cm, i.e. 0.3 m^2.

(a)

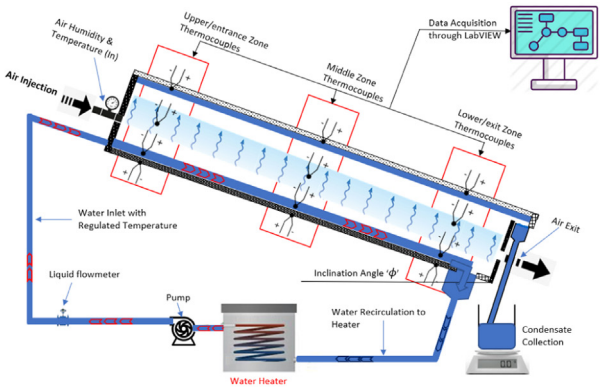

(b)

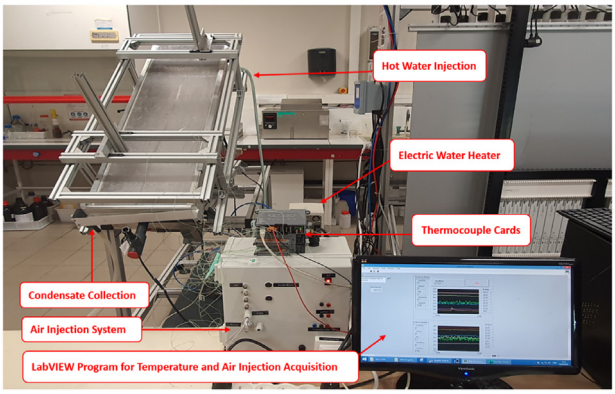

(c)

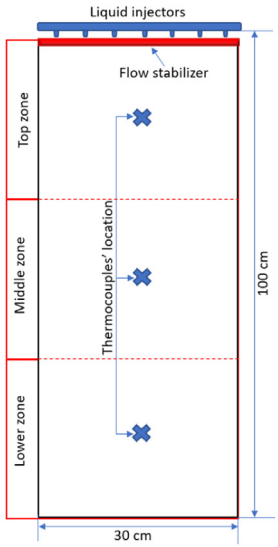

Fig. 1 – (a) Schematic description of indoor AlgoFilm ©. (b) Experimental setup for AlgoFilm © indoor prototype. (c) Flow for uniform film distribution and (d) Distribution of the thermocouples on sub-system "Flowing liquid".

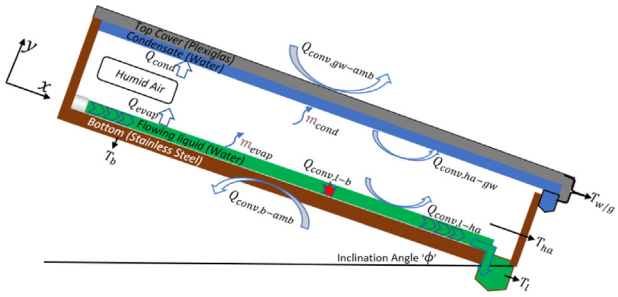

Fig. 2 – Graphical description of indoor model.

The interest of the indoor setup was to measure accurately the condensate mass flux. After reaching steady state the condensate mass was collected every hour, and every experiment was at least triplicated on same operating conditions (Inclination angle, liquid flow rate and temperature) and the mean data is considered for the averaged experimental condensation rate for each experiment.

3. Theoretical modeling

The mathematical model was developed for the prediction of heat and mass transfers involved in the passive thermal regulation technique of the Algofilm © photobioreactor.

All heat and mass fluxes are briefly illustrated in Fig. 2.

The following assumptions hold:

(i) The film flow is assumed to be at a constant velocity. The residence time of liquid is very short with respect to characteristic evaporation time, therefore the variation in the flowing film thickness is assumed to be negligible.

(ii) The temperature of the film is assumed to be constant throughout the process.

(iii) The overall system of the photobioreactor is subdivided into subsystems (bottom, liquid, humid air, condensate, glass), where each subsystem is characterized by its averaged temperature T_l, T_b, T_{ha}, $T_{w/g}$. It was assumed that the condensate and the glass are thermally thin body and characterized by the temperature $T_{w/g}$

(iv) The heat and mass conservation in each subsystem is assumed to be modeled by global balances, based on the variation in enthalpy of each subsystem. Therefore, the spatial average values were considered that is:

$$\frac{\partial \langle H_i \rangle}{\partial t} + \langle U_i \rangle \frac{\partial \langle H_i \rangle}{\partial x} = \sum Q_{in} - \sum Q_{out} \tag{1}$$

where $\langle H_i \rangle = H_{i,ref} + m_i cp_i T_i$ denotes the enthalpy of the subsystem $i = b, l, ha, g/w$. m_i, cp_i were respectively the mass and specific heat capacity of the subsystem i. Q_{in}, Q_{out} refers to input and output heat fluxes, respectively. $\langle U_i \rangle$ is the averaged velocity over thickness of each participating subsystem.

$$\langle U_i \rangle = \frac{1}{\delta_i} \int_0^{\delta_i} U_i(y,t)dy \quad \text{and} \quad \langle H_i \rangle = \frac{1}{\delta_i} \int_0^{\delta_i} H_i(x,y,t)dy \tag{2}$$

3.1. Heat balance equations

It should be observed that the momentum Equations are not included since it is assumed a constant mass flow rate and the coupling with the heat balance is achieved through the residence time.

(3) **Flowing Liquid:**
The liquid film thickness δ_l can be considered as constant over the length L of the PBR (smooth interface). The local energy Equation for a fully developped flow with an average velocity U_l, is expressed as follows:

$$\rho_l cp_l \frac{\partial T_l}{\partial t} + \rho_l cp_l \langle U_l \rangle \frac{\partial T_l}{\partial x} = k_l \frac{\partial^2 T_l}{\partial y^2} \qquad 0 < x < L, \quad 0 < y < \delta_l \tag{3}$$

where k_l is the thermal conductivity of the liquid, $T_l(x, y, t)$ is the temperature field of the liquid film. The transport mechanism with respect to the direction x is assumed to be purely advective, and purely diffusive in the y direction. Eq. (3) is subjected to the following initial and boundary conditions:

$$\begin{cases} T_l(x,y,t=0) = T_{l,0} \\ T_l(x=0,y,t) = T_{l,i} \\ k_l \left.\dfrac{\partial T_l}{\partial y}\right|_{y=0} = q_{conv,l-b} \\ k_l \left.\dfrac{\partial T_l}{\partial y}\right|_{y=\delta_l} = -q_{conv,l-ha} - q_{evap} \end{cases} \tag{4}$$

$S = L \times W$ is the surface of exchange. $T_{l,i}$ is the inlet temperature. $q_{conv,l-b}$ and $q_{conv,l-ha}$ are density of convective heat fluxes (W/m^2) between bottom-liquid, and liquid-humid air, respectively, and q_{evap} is the evaporation heat flux density.

The integration of Eq. (3) over the liquid film thickness leads to:

$$\rho_l cp_l \frac{\partial}{\partial t} \int_{y=0}^{\delta_l} T_l \; dy + \rho_l cp_l \langle U_l \rangle \int_{y=0}^{\delta_l} \frac{\partial T_l}{\partial x} dy = k_l \left(\left.\frac{\partial T_l}{\partial y}\right|_{y=\delta_l} - \left.\frac{\partial T_l}{\partial y}\right|_{y=0} \right) \tag{5}$$

The averaged temperature over the thickness of the liquid film reads as follows:

$$\langle T_l \rangle = \frac{1}{\delta_l} \int_0^{\delta_l} T_l(x,y,t)\, dy \tag{6}$$

The substitution of the boundary equations (4) and the averaged temperature over the thickness (6) into Eq. (5) gives:

$$\rho_l cp_l \delta_l \frac{\partial \langle T_l \rangle}{\partial t} + \rho_l cp_l \delta_l \langle U_l \rangle \frac{\partial \langle T_l \rangle}{\partial x} = -q_{conv,l-b} - q_{conv,l-ha} - q_{evap} \tag{7}$$

The integration of Eq. (5) over the length L gives the following equation:

$$\rho_l \delta_l cp_l \frac{d}{dt}\left[\int_{x=0}^{L} \langle T_l\rangle dx\right] + \rho_l \delta_l cp_l \langle U_l\rangle \left(\langle T_l\rangle|_{x=L} - \langle T_l\rangle|_{x=0}\right) = \int_{x=0}^{L} \left(-q_{conv,l-b} - q_{conv,l-ha} - q_{evap}\right) dx \quad (8)$$

The spatial average temperature of the flowing liquid, and the averaged heat fluxes over the surface of exchange are defined as follows:

$$\overline{T}_l = \frac{1}{L\ \ \delta_l}\left[\int_{x=0}^{L}\int_{y=0}^{\delta_l} T_l \ \ dxdy\right] \quad (9)$$

$$Q_i = W\int_{x=0}^{L} q_i dx \quad (10)$$

where $i = conv, l-b; conv, l-ha; evap$. The substitution of the averaged temperature and fluxes ((9, 10)) in Eq. (8) give the global energy equation of the flowing liquid.

$$m_l cp_l \frac{d\overline{T}_l}{dt} + \dot{m}_l cp_l \left(\langle T_l\rangle|_{x=L} - \langle T_l\rangle|_{x=0}\right) = \left(-Q_{conv,l-b} - Q_{conv,l-ha} - Q_{evap}\right) \quad (11)$$

where $\dot{m}_l = \rho_l \delta_l W \langle U_l\rangle$ is the mass flowrate of the liquid and $\dot{m}_l = \rho_l \delta_l WL$.
The characteristic time for heat exchange between the liquid and participating sub-systems i.e. (humid air and bottom) is defined as follows:

$$t_c = \frac{m_l cp_l}{S(h_{fc} + h_{cm} + h_{evap})} \quad (12)$$

The residence time can be defined as function of the average velocity $\langle U_l\rangle$ and the length of PBR as follows:

$$t_r = \frac{L}{\langle U_l\rangle} \quad (13)$$

When the residence time is smaller than the heat transfer characteristic time $t_r < t_c$, the heat flow is approximately equal to the heat exchanged between the liquid and the participating subsystems $\dot{m}_l cp_l \left(\langle T_l\rangle|_{x=L} - \langle T_l\rangle|_{x=0}\right) \approx -Q_{conv,l-b} - Q_{conv,l-ha} - Q_{evap}$. In such case the accumulation of the averaged sensible heat over the residence time is negligible, which allow to write $d\overline{T}_l/dt \approx 0$. Such approximation was experimentally verified (see Fig. 7b), since the liquid film residence time was short and the theoretical endorsement of $t_r < t_c$, the global modeling approach can be comfortably applied in the lab-scale Algofilm © . Therefore the Equation (11) can be re-written as:

$$\frac{dT_l}{dt} = 0 \quad (14)$$

(4) **Humid air:** The overall heat and mass transfer of the system are highly dependent on humid air as it is the main transporting medium between the flowing liquid and condensate film. The development of condensate film is highly dependent on this subsystem as it receives convective heat flux and mass from the flowing liquid and transports them to the condensate film. The global heat balance Eq. (1) in the case of humid air read as:

$$\frac{d\langle H_{ha}\rangle}{dt} + \langle U_{ha}\rangle \frac{d\langle H_{ha}\rangle}{dx} = Q_{evap} + Q_{conv,l-ha} - Q_{conv,ha-w} - Q_{cond} \quad (15)$$

where,

- $<U_{ha}>$ is the average velocity of the injection air (see Fig. 1a).
- $\langle H_{ha}\rangle = H_{ha,ref} + m_{ha} cp_{ha} T_{ha}$ is the enthalpy of the humid air.
- Q_{evap} is the evaporation heat flux.
- $Q_{conv,l-ha}$ is the convective heat flux between liquid and humid air.
- $Q_{conv,ha-w}$ is the convective heat flux between humid air and condensate film.
- Q_{cond} is the condensation heat flux.

One should note that some experiments were conducted without air injection which leads to reduction of Eq. (15) to:

$$\frac{d\langle H_{ha}\rangle}{dt} = Q_{evap} + Q_{conv,l-ha} - Q_{conv,ha-w} - Q_{cond} \quad (16)$$

(5) **Glass-condensate:** The condensate film development is mainly a function of vapour transported by humid air and condensed at the undersurface of the glass cover. The heat balance for condensate film is a function of heat and vapour transported from humid air to the glass and heat evacuated from the glass to the ambient air. In addition, an assumption of the thermally thin body was considered for the glass and condensate due to the small thickness of condensate film, accordingly, the global heat balance equation for this subsystem is written as follows:

$$\frac{d\langle H_{w/g}\rangle}{dt} = Q_{cond} + Q_{conv,ha-w} - Q_{conv,w-amb} \quad (17)$$

where,

- $\langle H_{w/g}\rangle = H_{w/g,ref} + (m_w cp_w + m_g cp_g) T_{w/g}$ is the enthalpy of the glass-condensate.
- $Q_{conv,ha-w}$ is the convective heat flux between condensate-glass and ambient air.

(6) **Bottom:** In the case of indoor Algofilm © bottom is exposed to the ambient atmosphere without having any insulation, therefore, it receives heat from flowing liquid in the form of forced convection and transfer heat to ambient atmosphere in the form of natural convection. The global heat balance equation (1) for the bottom will be rearranged as:

$$\frac{d\langle H_b\rangle}{dt} = Q_{conv,l-b} - Q_{conv,b-amb} \quad (18)$$

where

- $\langle H_b\rangle = H_{b,ref} + m_b cp_b T_b$ is the enthalpy of the bottom.
- $Q_{conv,l-b}$ is the forced convective heat flux between liquid and bottom.
- $Q_{conv,b-amb}$ is the convective heat flux between bottom and ambient air.

3.2. *Mass balance equation*

The mass transfer is mainly happening due to evaporation, and condensation. It is assumed saturated humid air and all

the vapour produced at the flowing liquid interface is condensed at the undersurface of the glass cover. The mass balance equation expressing the variation of m_w reads as follows:

$$\dot{m}_{ha}\Big|_{out} - \dot{m}_{ha}\Big|_{in} = \dot{m}_{evap} - \dot{m}_{w} \tag{19}$$

where $\dot{m}_{evap}$ is the evaporation rate, $\dot{m}_{ha}$ is the mass flow rate of the injected air. Without air injection Eq. (19) becomes:

$$\dot{m}_{w} = \dot{m}_{evap} \tag{20}$$

3.3. *Heat and mass transfer fluxes*

The heat and mass transfer model was developed by considering all significant transport fluxes including convective and latent heat transfers. The heat transfer in Algofilm © photobioreactor can be divided into two main categories internal and external heat transfers as shown in Fig. 1a. Internal heat transfer includes latent heat transfer (i.e. evaporation and condensation), and free/forced convection heat transfer between flowing liquid to humid air and bottom surface, and humid air to glass cover of Algofilm © . However, the external heat transfer is considered for the heat evacuated from the top cover and bottom surface to the ambient atmosphere by natural convection.

3.3.1. *Convective heat transfer fluxes*

The convective heat fluxes are described by Newton's law of cooling. The internal heat transfer coefficients are dependent on temperature and partial pressure of the vapour, due to the presence of simultaneous heat and mass transfer. However, the external heat transfer coefficients do not involve any mass transfer. The internal heat transfer fluxes are given by:

$$Q_{conv,l-ha} = Sh_{cm}\,(T_l - T_{ha}) \tag{21}$$

$$Q_{conv,ha-w} = Sh_{cha}\,(T_{ha} - T_w) \tag{22}$$

where S is the surface of the Algofilm © PBR and h_{cm}, h_{cha} are the heat transfer coefficients (from flowing liquid to humid air, humid air to condensate) and are theoretically derived by a heat and mass transfer analogy by Dunkle (1961), applied on solar photobioreactor Artu (2016) to quantify the free convective heat transfer in closed geometries. These coefficients are:

$$h_{cm} = 0.884\left[(T_l - T_w) + \left(\frac{p_{v,l} - p_{v,ha}}{2016 - p_{v,l}}\right)T_l\right]^{\frac{1}{3}} \tag{23}$$

$$h_{cha} = 0.884\left[(T_l - T_w) + \left(\frac{p_{v,ha} - p_{v,w}}{2016 - p_{v,l}}\right)T_l\right]^{\frac{1}{3}} \tag{24}$$

The heat transferred between the flowing liquid and the bottom is given by:

$$Q_{conv,l-b} = S\ \ h_{fc}\,(T_l - T_b) \tag{25}$$

where h_{fc} is the forced convective heat transfer coefficient and expressed as:

$$h_{fc} = \frac{Nuk_l}{L} \tag{26}$$

where k_l, L is the thermal conductivity of liquid and the length of the Algofilm © PBR, and Nu is the Nusselt number expressed as function of Re and Pr as follows Welty et al. (2014):

$$Nu = 0.664Re^{\frac{1}{2}}Pr^{\frac{1}{3}} \tag{27}$$

The amount of heat evacuated through external surfaces of Algofilm © PBR read as follows:

$$Q_{conv,b-amb} = S\ \ h_{b-amb}\,(T_b - T_{amb}) \tag{28}$$

$$Q_{conv,w-amb} = S\ \ h_{w/g-amb}\,(T_{w/g} - T_{amb}) \tag{29}$$

where h_{b-amb}, $h_{w/g-amb}$ are the heat transfer coefficients for the heat flow in upward and downward direction.

$$h_{b-amb} = \frac{Nu_b k_{air}}{L_c} \tag{30}$$

$$h_{w/g-amb} = \frac{Nu_{w/g} k_{air}}{L_c} \tag{31}$$

where k_{air} is the thermal conductivity of ambient air,L_c is the characteristic length of the heat exchanging surface and Nu_b, $Nu_{w/g}$ are the Nusselt numbers for natural convection for downward and upward heat flow respectively, which are the given as a function of Rayleigh number Ra.

$$Nu_b = 0.27Ra^{\frac{1}{4}} \tag{32}$$

$$Nu_{w/g} = 0.54Ra^{\frac{1}{4}} \tag{33}$$

3.3.2. *Latent heat transfer fluxes*

The latent heat fluxes of evaporation and condensation are given by the analogical expression of Newton's law of cooling but in terms of partial vapour pressures instead of temperatures of the participating subsystems. These fluxes are expressed as:

$$Q_{evap} = L_{evap}\dot{m}_{evap} \tag{34}$$

$$Q_{cond} = L_{evap}\dot{m}_{cond} \tag{35}$$

where L_{evap} is the latent heat of evaporation, and $\dot{m}_{evap}$, $\dot{m}_{cond}$ are the evaporation and condensation mass fluxes. In this case the humid air was assumed to be saturated with vapour, allowing then to write $\dot{m}_{evap} = \dot{m}_{cond}$ and $Q_{evap} = Q_{cond}$ Yu and Wang (2012).

3.3.3. *Mass transfer fluxes*

The evaporation mass flux $\dot{m}_{evap}$ is computed from:

$$\dot{m}_{evap} = S\ \ h_{evap}\,(p_{v,l} - p_{v,ha}) \tag{36}$$

where $p_{v,i}$ is the partial vapour pressure of subsystem $i = l, w/g$, and the mass transfer coefficient h_{evap} is obtained from the heat transfer coefficient h_{cm} (Eq. (23)) with a correlation factor of 9.15×10^{-7}, and is theoretically derived by a heat and mass transfer analogy by Dunkle (1961), applied on solar photobioreactor by Artu (2016) to quantify the evaporative heat transfer as follows:

$$h_{evap} = 9.15 \times 10^{-7} h_{cm} \tag{37}$$

3.4. *Numerical solution for heat and mass transfer model equations*

The substitution of all the above defined heat and mass fluxes and enthalpy expressions in equations ((14, 16),(17, 18),(20)) lead to system of five ODEs to be solved simultaneously as given in the following for the case of zero injected air flow:

$$\begin{cases} \dfrac{dT_l}{dt} = 0 \\ m_{air} cp_{air} \dfrac{dT_{ha}}{dt} = Q_{evap} + Q_{conv,l-ha} - Q_{conv,ha-w} - Q_{cond} \\ (m_w cp_w + m_g cp_g) \dfrac{dT_{w/g}}{dt} = Q_{cond} + Q_{conv,ha-w} - Q_{conv,w-amb} \\ m_b cp_b \dfrac{dT_b}{dt} = Q_{conv,l-b} - Q_{conv,b-amb} \\ \dfrac{dm_w}{dt} = S \quad h_{evap} (p_{v,l} - p_{v,ha}) \end{cases} \tag{38}$$

with the following initial conditions:

$$\begin{cases} T_l (t = 0) = T_{l,0} \\ T_{ha} (t = 0) = T_{ha,0} \\ T_{w/g} (t = 0) = T_{w/g,0} \\ T_b (t = 0) = T_{b,0} \\ m_w (t = 0) = 0 \end{cases} \tag{39}$$

The solution of heat and mass transfer model was obtained by integration with respect to time of the system of ordinary differential equations (38) taking into account the initial conditions (39). The integration of these ODEs was carried out by the MATLAB predefined function.

4. Results and discussions

The experimental and theoretical results are presented with different environmental and controlled operating conditions. The experimental results were also compared with the theoretical model in terms of condensed mass at the undersurface of the glass cover, and the temperatures of each subsystem.

4.1. *Experimental results*

The experiments were conducted by varying the inclination angle, flowing liquid temperature, and the air injection to evaluate the effect on hourly condensation rate, and the temperatures of each subsystem. The effect of inclination angle is a very important factor (Goshayeshi and Safaei, 2019) not only to see its impact but also to quantify the maximum experimental condensation rate. Fig. 3 shows the results for hourly condensation rate on a wide range of inclination angles 4–65 °, on fixed parameters such as liquid temperature (35, 40 and 50 °C) and flow rate of 0.08 l/s in the Algofilm © PBR.

The experimental results showed that the collection rate is increased with increasing ϕ up to a critical value $\phi = 35°$), where the collection rate reached the asymptotic value and revealed the experimental quantification of condensation rate. This fact was caused due to the increased gravitational force

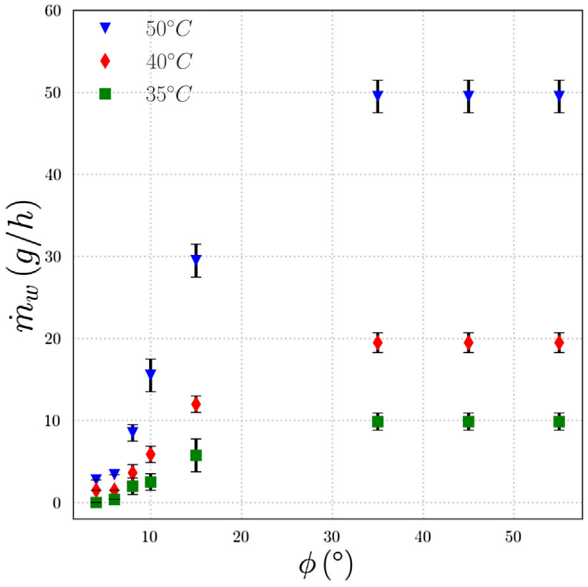

Fig. 3 – Effect of inclination angle on condensation rate.

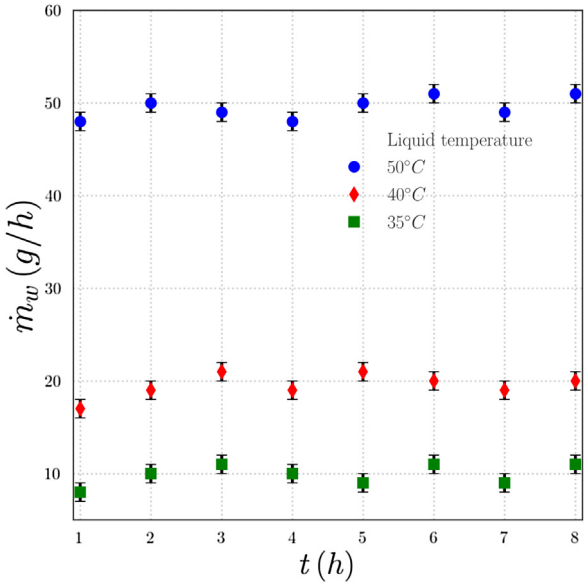

Fig. 4 – Effect of flowing liquid temperature on condensation rate for $\phi = 35°$.

which drives condensate to flow into the condensate collector (Goshayeshi and Safaei, 2019).

The influence of the flowing liquid temperature on the condensation rate is depicted in Fig. 4. The results showed that the condensation rate increased with the increasing flowing liquid temperature, where a large increase was observed from 9.5 g/h to 49.5 g/h on 35 and 50 °C respectively. This effect can be explained by the increase of transport of the vapour through buoyancy force which highly depends on the temperature gradient between flowing liquid and the glass cover. Moreover, the increase of the temperature of the flowing liquid also increased the partial pressure of the vapour at the interface, which results in the increase in evaporation as well as the condensation rate. This can help to correlate the indoor study with the outdoor atmosphere while dealing with the relevant temperature range.

Fig. 5 shows the photos taken from the top of the Algofilm © PBR for inclination angle of 6° at the temperature of 50 °C of the flowing liquid. These photos show the existence of polydisperse and connected droplets for all the cases considered.

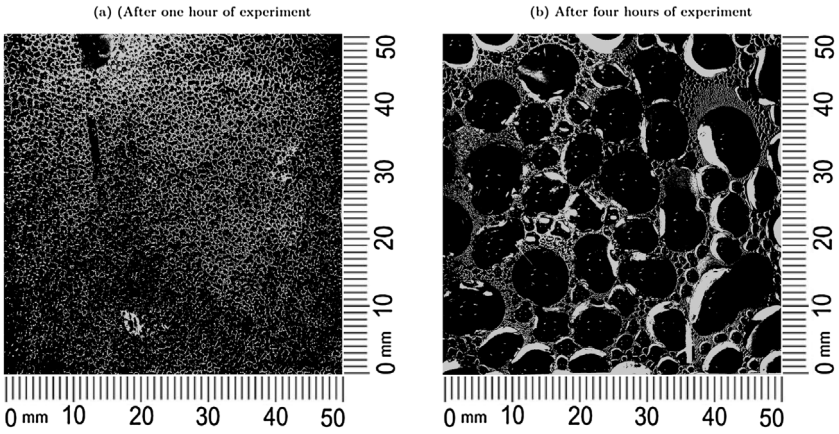

Fig. 5 – Development of irregular condensate film on $T_l = 50\,°C$ and $\phi = 6°$.

This observation made it possible to consider an irregular film of condensate at the undersurface of the glass cover.

The existence of irregular film made possible the estimation of an averaged condensate film on different inclination angles ϕ as shown in Fig. 5, calculated from the data of condensation rate experiments on different ϕ. The averaged condensate film thickness was calculated as follows:

$$\delta_{cond} = \frac{\dot{m}_w t_{d1}}{\rho_l \; S} \tag{40}$$

where δ_{cond} in the averaged film thickness, $\dot{m}_w$ is the maximum condensation rate (maximum condensation rate was collected by varying the inclination angles up to 65°, however after 35° the experimental condensation rate was constant, which allowed to assume that the condensation rate achieved at the critical inclination angle 35° is equivalent to the maximum experimental condensation rate and independent of ϕ), t_{d1} is the time taken by the first droplet to slide into the condensate collector, and S is the glass surface area. Furthermore, to estimate the averaged condensate film thickness the time between the initial time t_0 and the time when the first droplet to start slide t_{d1} was recorded, and the condensation rate was taken into account for the observed duration to compute the amount of condensate stocked at the under the surface of the top cover. The computed volume of condensate per surface area of glass cover gave the approximate averaged condensate film thickness.

Fig. 6 represents the averaged condensate film thickness estimated on the range of ϕ =4–35°. The maximum film thickness 2.2 mm was achieved on lowest ϕ of 4°, however, the film thickness remained minimum 0.1 mm on higher ϕ of 35°. The averaged condensate film thickness is highly dependent on inclination angle ϕ. If inclination angle ϕ is higher the condensate will continue to slide down into the condensate collector and less amount of condensate will remain on the undersurface of glass cover which leads the reduction in condensate film thickness. Nevertheless, when ϕ is lower as 4° the condensate could not slide into the collector and remained at the glass cover due to the least gravitational effect which results a significant condensate thickness as presented in Fig. 6, however sometimes droplets coalescence was observed due to short sliding of droplets, but that coalescence could not drive the condensate droplets into the collector. Such results showed the importance of the indoor experiments, which made possible, to estimate this condensate film thickness which was very difficult to obtain in outdoor conditions, where this information can be useful to estimate the filtering of infrared radiations.

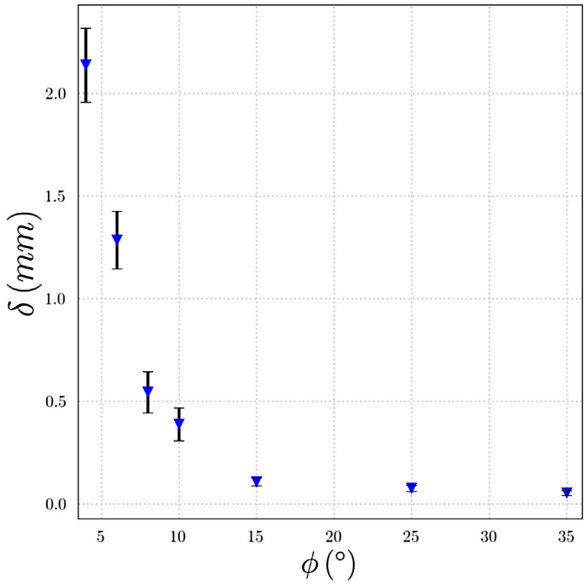

Fig. 6 – Estimation of averaged condensate film thickness over the range of inclination angles ϕ.

4.2. *Experimental validation of the theoretical assumptions*

The major assumptions made in the theoretical modeling include (i) natural convection in the humid air and (ii) uniform temperature within the subsystems. Accordingly, these assumptions were endorsed by the experimental results discussed hereafter.

It is well known that the influence of air injection in PBR is important for the microalgae as they require CO_2 injection for pH regulation and growth. From the point of view of heat and mass transfer, the air flow rate can influence the transport mechanism in the humid air, which can impact the condensation rate. To understand the impact of air injection on the transport behavior, experiments with different flow rates (i.e. 2.5–7.5 l/min) were conducted, while considering the airflow rate range of outdoor Algofilm © PBR i.e. 2–4 l/min. The vapour can be transported by air outside by forced convection reducing the amount of condensate on the undersurface glass cover. Fig. 7a represents the effect on condensation rate for different

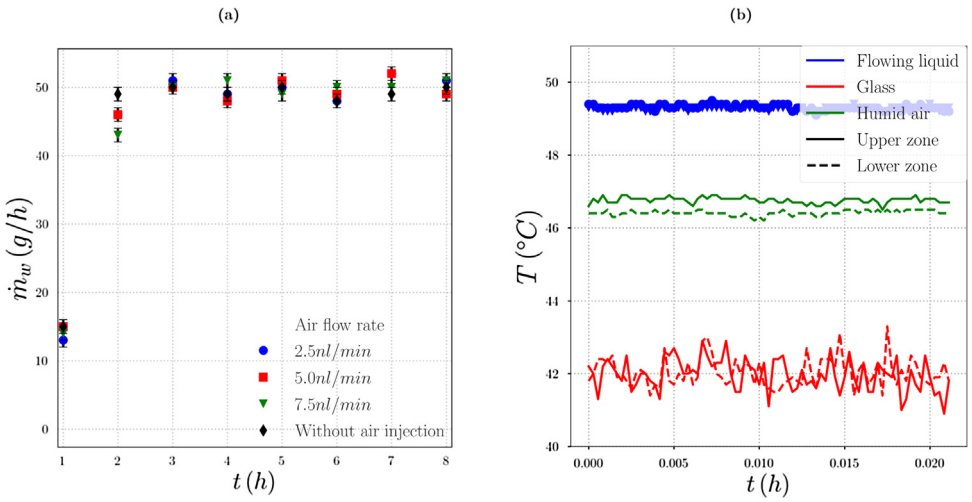

Fig. 7 – Experimental validation of theoretical assumptions: (a) Effect of air injection on condensation rate; (b) Temperature gradient of each subsystem for $T_l = 50\,°C$ (without air injection).

airflow rates form 2.5 to 7.5 l/min, a case without air injection was included as base of comparison.

Fig. 7a showed that natural convection dominated in Algofilm © PBR, therefore no any significant impact on the condensation rate was observed. Furthermore, it was also shown that the Richardson Number *Ri* for the air flow rates considered (2.5, 5, 7.5 l/min), had respectively the values (8440, 2110, 940), showing that the natural convection was the main heat transfer process. These results endorsed the assumption considered in the theoretical modeling that the dominated transport mechanism in humid air is natural convection.

Regarding the assumption of uniform temperature within each subsystem was also verified by measuring the temperature at entrance/upper zone and exit/ lower zone of the Algofilm © (see Fig. 1a), the comparison for each subsystem was depicted in Fig. 7b.

The results on Fig. 7b show that the gradient between the upper and lower zone is negligible. These results endorsed the global modeling approach for predicating heat and mass transfer in Algofilm © PBR. The assumption of uniform temperature within each subsystem was also discussed and validated experimentally by (Goetz et al., 2011). However in the large-scale outdoor PBR the temperature gradient may not be negligible, in such situation the local modeling approach is recommended. In the case of lab-scale Algofilm PBR the length and the height of flowing liquid are small enough to acquire the temperature gradient within the flowing liquid film as it is controlled through and external water heater, and the residence time is very short.

4.3. *Theoretical results and comparison with experiments*

The validation of the simulated results consists of the comparison with the experimental results for temperature, averaged mass transfer flux and the condensed mass. The comparison was made for the temperature of humid air, condensate/glass, and the bottom of Algofilm © PBR.

The solution of Eqs. (38) for indoor conditions allowed to predict the temperatures of each subsystem and condensate amount at the undersurface of the glass cover. The simulations were carried out on three liquid temperatures 35, 40, and 50 °C as reported in Fig. 8. For all the cases considered, the evolution of the temperature of each subsystem showed transient behaviour in the first hour before reaching steady-state. The simulated results were in a good agreement with the experimental results for all the investigated temperatures. Whereas the maximum deviation at the steady-state was observed at most 1 °C. However, considering the complexities of the simultaneous heat and mass transfer with phase change phenomena and the global model this deviation is acceptable. Furthermore, from the point of view of microalgae growth and temperature modeling studies this deviation will not have a significant effect (Pruvost et al., 2019).

Fig. 10a represents the evolution of experimental and numerical condensed mass for different temperature of flowing liquid i.e ($T_l = 35$, 40, 50 °C). The evolution of m_w over the time exhibited linear behaviour after achieving steady-state for all the temperatures of flowing liquid considered. The comparison of results is in acceptable range with a maximum deviation of 2 g/h for 50 °C, but for lower temperatures which represent the actual range for microalgae production about 20–30 °C, the modeling results are in very good agreement with a maximum deviation 0.8 g/h.

The linear behaviour of condensed mass over time allowed us to calculate the averaged condensation rate with respect to the liquid temperature. Fig. 10b represents the comparison of experimental and simulation results of averaged condensation rate for all the investigated temperatures. The mass flux is seeming to be a highly dependent on the flowing liquid temperature as it increased from 10 g/h to 49.5 g/h by varying the temperature from 35 to 50 °C.

Fig. 9 shows the evolution of heat fluxes i.e. evaporation and condensation over the range of studied flowing liquid temperature (35, 40, and 50 °C) with respect to time. The humid air between flowing liquid (evaporating surface) and top cover (condensing surface) was assumed to be instantaneously saturated with vapour in this case, therefore all the vapour produced at the liquid/air interface will be condensed at under surface of the top cover, since the PBR is closed. This assumption was justified for a similar case through lattice Boltzmann simulations, accordingly the latent heat of evaporation and condensation are same, since $m_{evap} = m_{cond}$ (Yu and Wang, 2012). The maximum value for evaporation and condensation heat fluxes after reaching fully developed condition is about 21.9, 39.19, 89.65 w/m^2 for (35, 40, 50 °C), respectively. The driven force for evaporation and condensation is the temperature difference between the flowing liquid

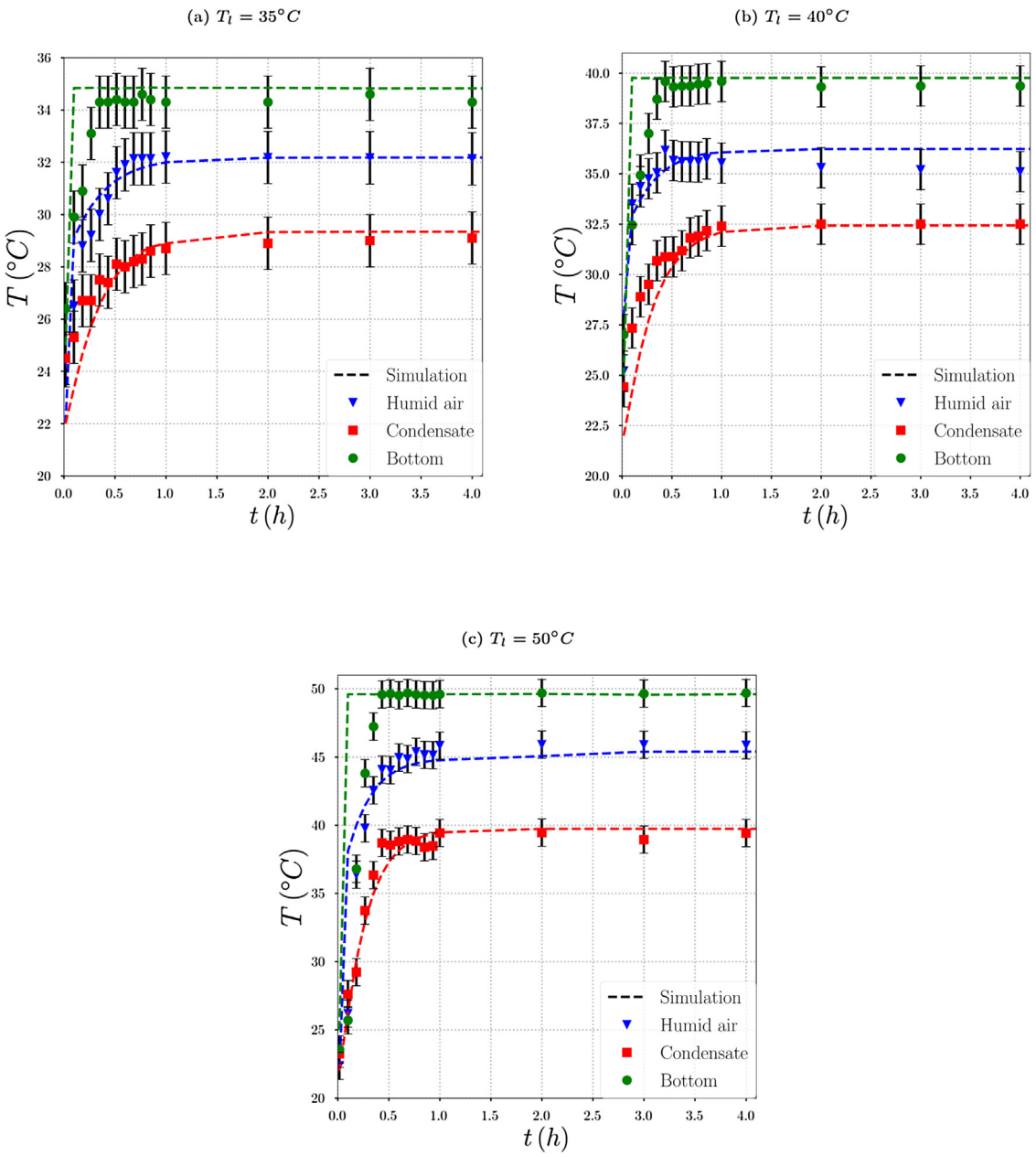

Fig. 8 – Comparaison between simulated and experimental temperature of each subsystem for $T_l = 35, 40, 50\,°C$.

(which is controlled through water heater) and the ambient temperature (regulated indoor temperature). Therefore, at the start of simulation the magnitude of these fluxes is higher because of the large temperature gradient as the initial conditions for liquid temperature are (35, 40, 50 °C), however the indoor ambient temperature is almost constant at 23 °C which also corresponds to the humid air temperature experimentally as well as numerically at initial conditions. The transient time for simulation or experiments is maximumly about one hour for studied range of temperature as shown in Fig. 8, which caused higher values for evaporation and condensation fluxes for first hour but declining continuously. This decline in the heat fluxes is due to decrease in the temperature difference (between flowing liquid and humid air) which was maximum at initial conditions, however after reaching fully developed conditions (after one hour) these fluxes became constant as the temperature gradient between humid air and flowing liquid reached at a constant value (numerically as well as experimentally).

The evolution of averaged condensation rate over the range of liquid temperature is presented in Fig. 11 which shows the same trend of as Fig. 10b, where the increase in liquid temperature results an increase in averaged condensation rate. This figure also shows a critical temperature for which no condensation was observed, that corresponds perfectly to the ambient temperature. As expected, this result seems to be logical while there is no temperature gradient which is driving force for evaporation, therefore the system has achieved thermal equilibrium. Such ascertainment shows the impact of the ambient temperature on evaporation which was not so expected even when the liquid temperature is automatically regulated. This result was further studied to see the impact of ambient temperature on the condensation rate and some simulations were carried out by considering the ambient indoor temperature variation. The results of these simulations exhibited that the ambient temperature can also be an influencing parameter for condensation rate, as it was significantly influenced by these small temperature deviations i.e. (23 ± 2 °C).

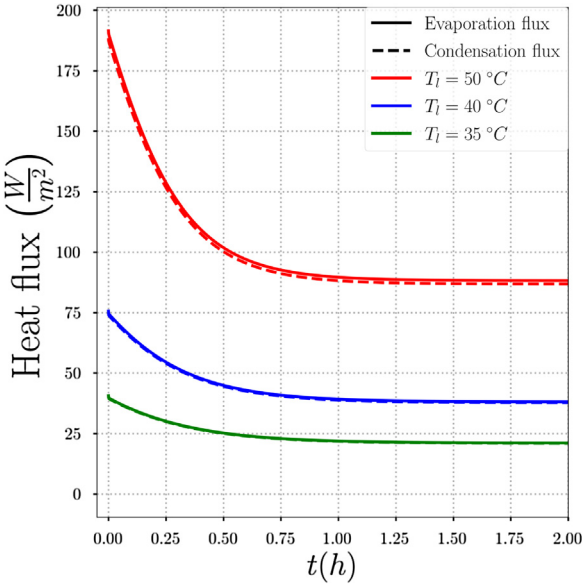

Fig. 9 – Evolution of evaporation and condensation latent heat fluxes for $T_l = 35, 40, 50\,°C$.

The influence of flowing liquid and ambient temperatures can be stretched to develop a correlation to estimate the condensation rate for closed PBRs in realistic conditions. Liu et al. (2019) showed that the mass flux of an evaporating liquid film can be proportional to the mass flux derived from the analytical solution of Stefan flow transport Equation in binary gas mixture, which is expressed as follows:

$$\dot{m} = \beta \times \frac{S\rho_{air}D_v}{\delta_a ir} \ln\left(\frac{1 - Y_{v,amb}}{1 - Y_{v,l}}\right) \tag{41}$$

where:

- $Y_{v,l}, Y_{v,\infty}$ are the mass fraction of vapor in liquid and gas respectively, β is the factor of proportionality, and δ_{air} is the thickness air gap.
- D_v is the binary diffusion coefficient, which can be expressed in this case as a function of the flowing liquid temperature by the relation of Fuller–Schettler–Giddings (Green and Perry, 2019):

$$D_v = \frac{10^{-7} T_l^{1.75} \sqrt{\frac{1}{M_a} + \frac{1}{M_v}}}{P_{amb}\left(\nu_a^{1/3} + \nu_v^{1/3}\right)} \tag{42}$$

  where $M_i, i = a, v$ is the molecular mass for air and vapor and ν_i is the diffusion volumes for air and vapor molecules.
- ρ_{air} is the density of vapor evaluated at the liquid temperature, which can be expressed by the perfect gas law as follows:

$$\rho_{air} = \frac{P_{amb}M_{air}}{\hat{R}T_{amb}} \tag{43}$$

The influencing parameters of the evaporation flux (Liu et al., 2019) are the temperatures of the evaporating liquid film and the gas. However in current study the driving force of evaporation is the temperature gradient between the flowing liquid film and ambient air, accordingly the mass flux in current study can be expressed in same way as Eq. (41), therefore a simulation was carried out by considering ambient air temperature as 23 °C and results are plotted in Fig. 12, where the mass

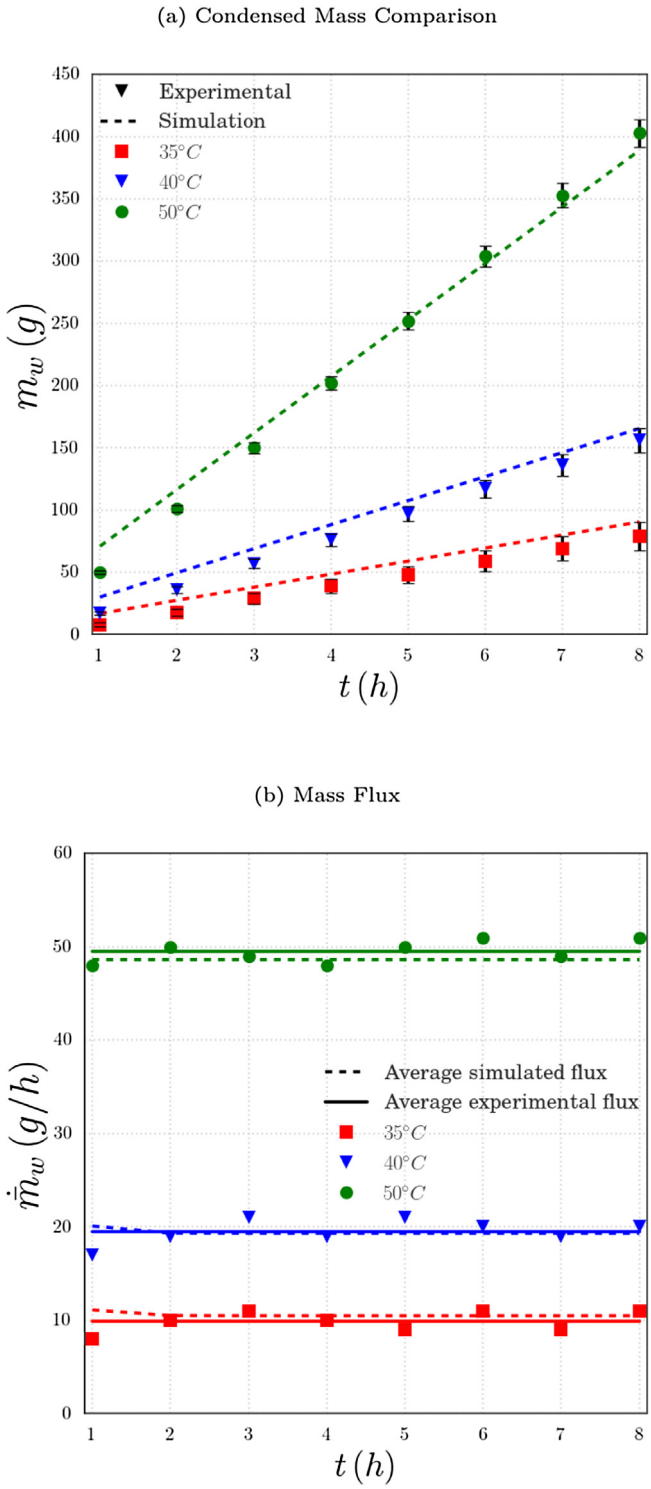

Fig. 10 – Comparison of experimental and simulated results for $T_l = 35, 40, 50\,°C$: (a) Condensed mass (b) Mass flux.

flux given by Eq. (41) showed the same trend with simulation results, while considering a constant of proportionality $\beta = 98$. However, the constant of proportionality β appeared as a function of ambient air temperature when some simulations were carried out by considering the wide ange of ambient temperature with respect to seasonal variations. Therefore, to extend the applicability the developed correlation β was fitted as func-

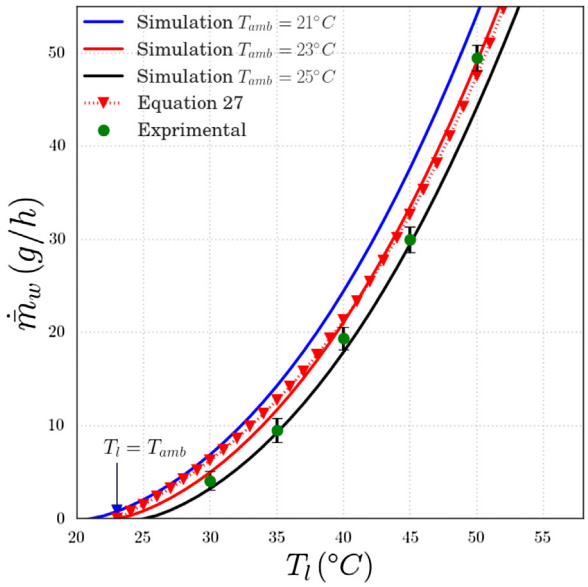

Fig. 11 – Evolution of condensation rate as a function of flowing liquid and ambient temperature.

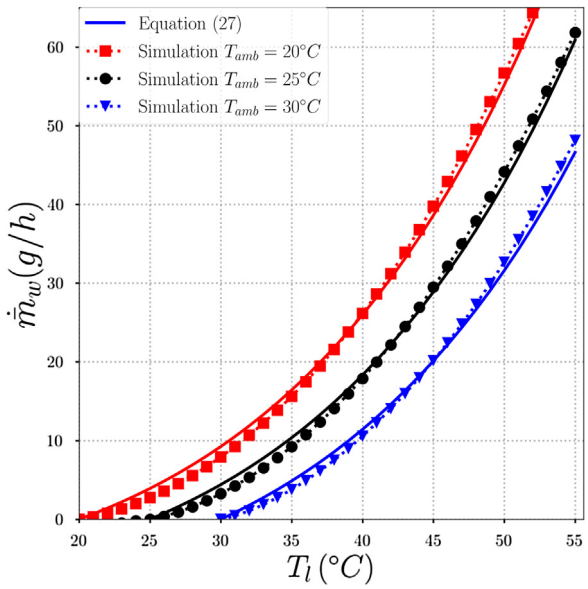

Fig. 12 – Evolution average condensation rate as a function of ambient temperature (comparison of developed correlation with simulations).

tion of ambient air temperature, which leads to the following expression:

$$\beta = 2.011 \left(\frac{T_{amb}}{T_K}\right)^2 - 5.168 \frac{T_{amb}}{T_K} + 3.335 \quad (44)$$

$T_K = 273.15$ K is the absolute temperature.

This correlation takes into account the temperature of the flowing liquid and the ambient air. These temperatures, in outdoor conditions, are always varying with respect to the weather conditions, which may allow to predict the mass of condensed water on the undersurface of the glass cover of Algofilm © PBR, which is very important to quantify the infrared filtration. Fig. 12 showed the comparison of results of simulation and Eq. (41) for average condensation rate with respect to T_l. The comparison showed that the correlation can be applied to predict the condensation rate over the wide range of ambient temperature, which will be of great interest in outdoor conditions.

4.4. *Validation of the indoor model in a simulated sunny day*

Fig. 13a and b are showing the evolution in simulated sunny day experiment and simulation for the temperatures of different sub-systems and the condensed mass, respectively.

In order to test the response of the developed heat and mass transfer model on dynamic conditions, a mimic experiment was conducted to validate the model on a representative condition of a typical outdoor day, by varying liquid temperature using an external water heater. Flowing liquid temperature was increased from 35 °C up to 50 °C and then decreased inversely with a time interval of one hour by considering the thermal inertia of solar radiation in a typical sunny day. This approach of simulated sunny day with artificial solar light was also considered by Goetz et al. (2011) in controlled indoor conditions for the validation of heat transfer model to predict the temperatures of the different subsystems.

The simulated results for temperature predictions of each subsystem (without any fitting or adjustment) were compared with the experimental ones and showed a good agreement (see Fig. 13a). In addition to temperature validation, the condensed mass prediction was also in good agreement (Fig. 13b) over the period of mimic outdoor day. The experimental mass collected over the period of whole experiment was 95 g, however the deviation of 15 g was observed at the end of experiment but that corresponds to the mass remained at the glass cover before the sliding of the first droplet as discussed in Fig. 6. These results showed the capability of developed model to be applied on real outdoor solar conditions.

Goetz et al. (2011) carried out some outdoor experiments and the mean temperature of flowing liquid reached up to 55 °C in a typical sunny day in the month of July, but in the current study it is experimentally and numerically revealed that evaporation rate at this temperature can easily reached around 65 g/h (see Fig. 11), which is not a negligible value. The condensed water mass can serve the purpose of passive evaporating cooling and filtration of infrared spectrum to avoid overheating of microalgae culture with a passive approach. Indeed, Nwoba et al. (2019) have shown the influence of the infrared filtration on microalgae culture temperature, where passive evaporating cooling was used as a filter for infrared radiation to avoid the overheating of microalgae and temperature reduction of 8 °C was observed when compared with and without PEC. This fact endorsed the need of incorporation of simultaneous heat and mass transfer model for thermal regulation of Algofilm © PBR.

5. Conclusion

The present work was aimed to develop a simultaneous heat and mass transfer model to predict the condensate film thickness which will absorb the Infrared spectrum (main source of overheating). The interest of the indoor study was to validate the model with controlled operating parameters (not possible in outdoor conditions) and experimentally investigating all the influencing parameters for evaporation and condensation. Accordingly, a detailed experimental and theoretical

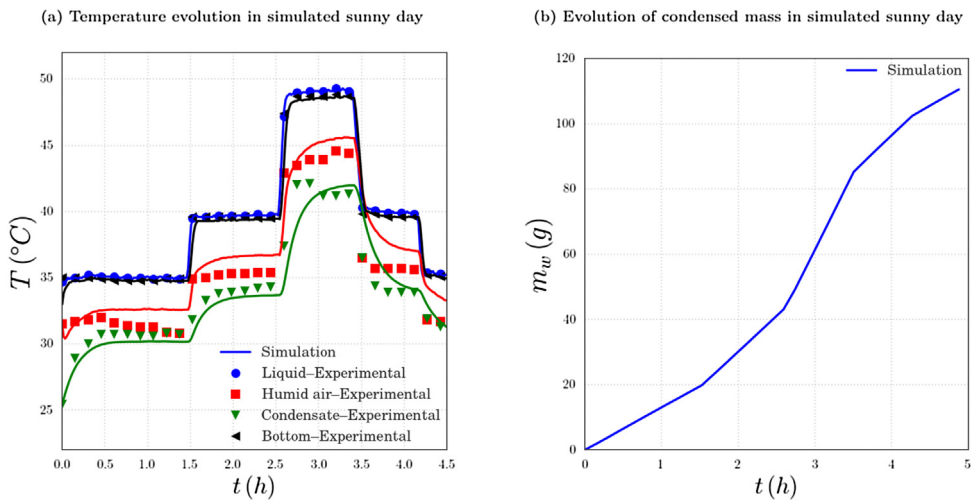

Fig. 13 – Evolution of condensed mass and temperatures of each sub-system in simulated sunny day.

study on lab-scale has been conducted. The experimental study focused on the evolution of temperature and condensed mass as a function of inclination angle, air injection, flowing liquid and ambient temperature. The results showed that the temperature of flowing liquid is the most important factor on condensation rate, whereas the air injection has not shown any significant effect for the investigated range.

These results revealed that air injection in outdoor condition will not affect the transport of heat and mass by natural convection. The numerical results were carried out for the prediction of temperature and condensed for the wide range of flowing liquid temperatures i.e. 30–50 °C. The experimental and numerical results were found in a good agreement for the whole range of flowing liquid temperature in steady state conditions. Besides, the model has the ability to predict the temperature and condensed mass on artificial dynamic condition. The good agreement between numerical and experimental results made possible to develop a correlation to estimate the condensation rate as a function the flowing liquid and ambient temperature; the latter appeared to be important in the evaporation process.

The water is the potential filter for the infrared spectrum (main source of overheating the microalgae). Active cooling systems such as passive evaporating cooling system is not viable due to the water constraints, therefore the developed passive thermal regulation approach will serve both purposes: (i) do not need any fresh water to filter infrared spectrum as reported by Krauter (2004), Nwoba et al. (2019), Ghosal et al. (2020); (ii) condensate film development will be a function of solar irradiation intensity (condensation would be maximum at the peak hours of the day which will filter infrared radiations since the present indoor study showed that the evaporation rate is a function of flowing liquid and ambient temperatures). The development of current simultaneous heat and mass transfer model with a good agreement on a simulated sunny will be a prime step to apply this model on real solar conditions, where the estimation of condensed mass is essential to quantify the amount of filtered infrared radiations.

Declaration of Competing Interest

The authors report no declarations of interest.

Acknowledgment

The Higher Education Commission, Pakistan is acknowledged for the financial support to the PhD student under their project HEC-UESTP, Pakistan.

References

Al Ketife, A.M., Judd, S., Znad, H., 2016. A mathematical model for carbon fixation and nutrient removal by an algal photobioreactor. Chem. Eng. Sci. 153, 354–362, http://dx.doi.org/10.1016/j.ces.2016.07.042.

Apel, A., Pfaffinger, C., Basedahl, N., Mittwollen, N., Göbel, J., Sauter, J., Brück, T., Weuster-Botz, D., 2017. Open thin-layer cascade reactors for saline microalgae production evaluated in a physically simulated mediterranean summer climate. Algal Res. 25, 381–390, http://dx.doi.org/10.1016/j.algal.2017.06.004.

Apel, A.C., Weuster-Botz, D., 2015. Engineering solutions for open microalgae mass cultivation and realistic indoor simulation of outdoor environments. Bioprocess Biosyst. Eng. 38, 995–1008, http://dx.doi.org/10.1007/s00449-015-1363-1.

Artu, A., 2016. Etude et optimisation de la culture de microalgues en photobioréacteurs solaires, Ph. D. thesis. PhD Thesis. University of Nantes.

Axelsson, L., Franzén, M., Ostwald, M., Berndes, G., Lakshmi, G., Ravindranath, N.H., 2012. Perspective: Jatropha cultivation in southern India: Assessing farmers' experiences. Biofuels Bioprod Biorefining 6, 246–256, http://dx.doi.org/10.1002/bbb.1324.

Baer, S., Heining, M., Schwerna, P., Buchholz, R., Hübner, H., 2016. Optimization of spectral light quality for growth and product formation in different microalgae using a continuous photobioreactor. Algal Res. 14, 109–115, http://dx.doi.org/10.1016/j.algal.2016.01.011.

Bechet, Q., 2014. Modelling the impact of temperature on microalgae productivity during outdoor cultivation, Ph. D. thesis. Massey University.

Béchet, Q., Shilton, A., Fringer, O.B., Munoz, R., Guieysse, B., 2010. Mechanistic modeling of broth temperature in outdoor photobioreactors. Environ. Sci. Technol. 44, 2197–2203, http://dx.doi.org/10.1021/es903214u.

Béchet, Q., Shilton, A., Guieysse, B., 2014. Full-scale validation of a model of algal productivity. Environ. Sci. Technol. 48, 13826–13833, http://dx.doi.org/10.1021/es503204e.

Benemann, J., 2013. Microalgae for biofuels and animal feeds. Energies 6, 5869–5886, http://dx.doi.org/10.3390/en6115869.

Cheng, J., Lai, X., Ye, Q., Guo, W., Zhou, J., 2020. Numerical simulation on optimizing flow field and flashing-light effect in jet-aerated tangential swirling-flow plate photobioreactor to improve microalgal growth. Chem. Eng. Sci. 215, 115371, http://dx.doi.org/10.1016/j.ces.2019.115371.

Deprá, M.C., Mérida, L.G., de Menezes, C.R., Zepka, L.Q., Jacob-Lopes, E., 2019. A new hybrid photobioreactor design for microalgae culture. Chem. Eng. Res. Design 144, 1–10, http://dx.doi.org/10.1016/j.cherd.2019.01.023.

Derakhshan, Z., Ehrampoush, M.H., Mahvi, A.H., Dehghani, M., Faramarzian, M., Eslami, H., 2019. A comparative study of hybrid membrane photobioreactor and membrane photobioreactor for simultaneous biological removal of atrazine and CNP from wastewater: A performance analysis and modeling. Chem. Eng. J. 355, 428–438, http://dx.doi.org/10.1016/j.cej.2018.08.155.

Draaisma, R.B., Wijffels, R.H., Slegers, P.M.E., Brentner, L.B., Roy, A., Barbosa, M.J., 2013. Food commodities from microalgae. Curr. Opin. Biotechnol. 24, 169–177, http://dx.doi.org/10.1016/j.copbio.2012.09.012.

Dunkle, R., 1961. Solar water distillation: the roof type still and a multiple effect diffusion still. In: in: Proc. International Heat Transfer Conference. University of Colorado, USA, pp. 895.

Ghosal, M., Sethi, A., Behera, D., 2020. Performance of solar photovoltaic module through combined air and water cooling in warm and humid climatic condition of India. MATTER: Int. J. Sci. Technol., 6, http://dx.doi.org/10.20319/mijst.2020.61.1525.

Goetz, V., Borgne, F.L., Pruvost, J., Plantard, G., Legrand, J., 2011. A generic temperature model for solar photobioreactors. Chem. Eng. J. 175, 443–449, http://dx.doi.org/10.1016/j.cej.2011.09.052.

Goshayeshi, H.R., Safaei, M.R., 2019. Effect of absorber plate surface shape and glass cover inclination angle on the performance of a passive solar still. Int. J. Numer. Methods Heat Fluid Flow 30, 3183–3198, http://dx.doi.org/10.1108/HFF-01-2019-0018.

Green, D.W., Perry, R.H., 2019. Perry's Chemical Engineers' Handbook/edición Don W. Green y Robert H. Perry. C 660.28 P47 2008.

Hindersin, S., Leupold, M., Kerner, M., Hanelt, D., 2013. Irradiance optimization of outdoor microalgal cultures using solar tracked photobioreactors. Bioprocess Biosyst. Eng. 36, 345–355, http://dx.doi.org/10.1007/s00449-012-0790-5.

Huesemann, M., Dale, T., Chavis, A., Crowe, B., Twary, S., Barry, A., Valentine, D., Yoshida, R., Wigmosta, M., Cullinan, V., 2017. Simulation of outdoor pond cultures using indoor led-lighted and temperature-controlled raceway ponds and phenometrics photobioreactors. Algal Res. 21, 178–190, http://dx.doi.org/10.1016/j.algal.2016.11.016.

de Jesus, S.S., Maciel Filho, R., 2017. Potential of algal biofuel production in a hybrid photobioreactor. Chem. Eng. Sci. 171, 282–292, http://dx.doi.org/10.1016/j.ces.2017.05.041.

Kirk, J.T., 1988. Solar heating of water bodies as influenced by their inherent optical properties. J. Geophys. Res.: Atmospheres 93, 10897–10908, http://dx.doi.org/10.1029/JD093iD09p10897.

Krauter, S., 2004. Increased electrical yield via water flow over the front of photovoltaic panels. Solar Energy Mater. Solar Cells 82, 131–137, http://dx.doi.org/10.1016/j.solmat.2004.01.011.

Le Borgne, F., 2014. Développement d'un photobioréacteur solaire intensifié en vue de la production à grande échelle de biomasse microalgale, Ph. D. thesis. PhD Thesis. University of Nantes.

Litchman, E., Klausmeier, C.A., 2001. Competition of phytoplankton under fluctuating light. Am. Naturalist 157, 170–187, http://dx.doi.org/10.1086/318628.

Liu, H., Jia, M., Cai, C., Zhang, Y., et al., 2019. An analytical model of the heating and evaporation of bi-component wall film. Int. Commun. Heat Mass Transfer 105, 28–36, http://dx.doi.org/10.1016/j.icheatmasstransfer.2019.03.014.

Luo, Y., Logan, A., Henderson, R.K., Le-Clech, P., 2021. Evaluating the resilience of photobioreactors in response to hazardous chemicals. Chem. Eng. J. 405, 126666, http://dx.doi.org/10.1016/j.cej.2020.126666.

Mata, T.M., Martins, A.A., Caetano, N.S., 2010. Microalgae for biodiesel production and other applications: a review. Renew. Sustain. Energy Rev. 14, 217–232, http://dx.doi.org/10.1016/j.rser.2009.07.020.

Moheimani, N.R., Isdepsky, A., Lisec, J., Raes, E., Borowitzka, M.A., 2011. Coccolithophorid algae culture in closed photobioreactors. Biotechnol. Bioeng. 108, 2078–2087, http://dx.doi.org/10.1002/bit.23161.

Nwoba, E.G., Ayre, J.M., Moheimani, N.R., Ubi, B.E., Ogbonna, J.C., 2016. Growth comparison of microalgae in tubular photobioreactor and open pond for treating anaerobic digestion piggery effluent. Algal Res. 17, 268–276, http://dx.doi.org/10.1016/j.algal.2016.05.022.

Nwoba, E.G., Parlevliet, D.A., Laird, D.W., Vadiveloo, A., Alameh, K., Moheimani, N.R., 2019. Can solar control infrared blocking films be used to replace evaporative cooling for growth of Nannochloropsis sp. in plate photobioreactors? Algal Res. 39, 101441, http://dx.doi.org/10.1016/j.algal.2019.101441.

Pruvost, J., Cornet, J., Goetz, V., Legrand, J., 2012. Theoretical investigation of biomass productivities achievable in solar rectangular photobioreactors for the cyanobacterium arthrospira platensis. Biotechnol. Progress 28, 699–714, http://dx.doi.org/10.1002/btpr.1540.

Pruvost, J., Goetz, V., Artu, A., Das, P., Jabri, H.A., 2019. Thermal modeling and optimization of microalgal biomass production in the harsh desert conditions of State of Qatar. Algal Res. 38, 101381, http://dx.doi.org/10.1016/j.algal.2018.12.006.

Pruvost, J., Le Borgne, F., Artu, A., Cornet, J.F., Legrand, J., 2016. Industrial photobioreactors and scale-up concepts. Adv. Chem. Eng., Elsevier 48, 257–310, http://dx.doi.org/10.1016/bs.ache.2015.11.002.

Pruvost, J., Le Borgne, F., Artu, A., Legrand, J., 2017. Development of a thin-film solar photobioreactor with high biomass volumetric productivity (AlgoFilm©) based on process intensification principles. Algal Res. 21, 120–137, http://dx.doi.org/10.1016/j.algal.2016.10.012.

Pruvost, J., Pottier, L., Legrand, J., 2006. Numerical investigation of hydrodynamic and mixing conditions in a torus photobioreactor. Chem. Eng. Sci. 61, 4476–4489, http://dx.doi.org/10.1016/j.ces.2006.02.027.

Ras, M., Steyer, J.P., Bernard, O., 2013. Temperature effect on microalgae: a crucial factor for outdoor production. Rev. Environ. Sci. Biotechnol. 12, 153–164, http://dx.doi.org/10.1007/s11157-013-9310-6.

Sabri, L.S., Sultan, A.J., Al-Dahhan, M.H., 2019. Investigating the cross-sectional gas holdup distribution in a split internal-loop photobioreactor during microalgae culturing using a sophisticated computed tomography (ct) technique. Chem. Eng. Res. Design 149, 13–33, http://dx.doi.org/10.1016/j.cherd.2019.06.017.

Shuba, E.S., Kifle, D., 2018. Microalgae to biofuels: 'Promising' alternative and renewable energy, review. Renew. Sustain. Energy Rev. 81, 743–755, http://dx.doi.org/10.1016/j.rser.2017.08.042.

Singh, S., Singh, P., 2015. Effect of temperature and light on the growth of algae species: a review. Renewable and sustainable energy reviews 50, 431–444, http://dx.doi.org/10.1016/j.rser.2015.05.024.

Solimeno, A., Gabriel, F., García, J., 2017. Mechanistic model for design, analysis, operation and control of microalgae cultures: calibration and application to tubular photobioreactors. Algal Res. 21, 236–246, http://dx.doi.org/10.1016/j.algal.2016.11.023.

Spolaore, P., Joannis-Cassan, C., Duran, E., Isambert, A., 2006. Commercial applications of microalgae. Journal of Bioscience and Bioengineering 101, 87–96, http://dx.doi.org/10.1263/jbb.101.87.

Torzillo, G., Pushparaj, B., Bocci, F., Balloni, W., Materassi, R., Florenzano, G., 1986. Production of spirulina biomass in closed photobioreactors. Biomass 11, 61–74, http://dx.doi.org/10.1016/0144-4565(86)90021-1.

Ugwu, C.U., Aoyagi, H., Uchiyama, H., 2008. Photobioreactors for mass cultivation of algae. Bioresour. Technol. 99, 4021–4028, http://dx.doi.org/10.1016/j.biortech.2007.01.046.

Welty, J., Rorrer, G.L., Foster, D.G., 2014. Fundamentals of Momentum, Heat, and Mass Transfer. John Wiley & Sons.
Wondraczek, L., Tyystjärvi, E., Méndez-Ramos, J., Müller, F.A., Zhang, Q., 2015. Shifting the Sun: solar spectral conversion and extrinsic sensitization in natural and artificial photosynthesis. Adv. Sci. 2, 1–13, http://dx.doi.org/10.1002/advs.201500218.
Xie, B., Gong, W., Tang, X., Bai, L., Guo, Y., Wang, J., Zhao, J., Fan, Y., Li, G., Liang, H., 2019. Blending high concentration of anaerobic digestion effluent and rainwater for cost-effective Chlorella vulgaris cultivation in the photobioreactor. Chem. Eng. J. 360, 861–865, http://dx.doi.org/10.1016/j.cej.2018.12.009.
Xu, L., Weathers, P.J., Xiong, X.R., Liu, C.Z., 2009. Microalgal bioreactors: Challenges and opportunities. Eng. Life Sci. 9, 178–189, http://dx.doi.org/10.1002/elsc.200800111.
Yang, Z., Nie, C., Hou, Q., Zhang, L., Zhang, S., Yu, Z., Pei, H., 2019. Coupling a photosynthetic microbial fuel cell (PMFC) with photobioreactors (PBRs) for pollutant removal and bioenergy recovery from anaerobically digested effluent. Chem. Eng. J. 359, 402–408, http://dx.doi.org/10.1016/j.cej.2018.11.136.
Yu, J., Wang, H., 2012. A molecular dynamics investigation on evaporation of thin liquid films. Int. J. Heat Mass Transfer 55, 1218–1225, http://dx.doi.org/10.1016/j.ijheatmasstransfer.2011.09.035.
Zhao, L., Zeng, G., Gu, Y., Tang, Z., Wang, G., Tang, T., Shan, Y., Sun, Y., 2019. Nature inspired fractal tree-like photobioreactor via 3D printing for CO2 capture by microaglae. Chem. Eng. Sci. 193, 6–14, http://dx.doi.org/10.1016/j.ces.2018.08.057.